Pulse Radiolysis of Supercritical Water. 1. Reactions between Hydrophobic and Anionic Species†

Jason Cline, Kenji Takahashi,‡ Timothy W. Marin, Charles D. Jonah, and David M. Bartels*

Chemistry Division, Argonne National Laboratory, Argonne, Illinois 60439

Received: September 18, 2002

Reaction rates of solvated electrons with oxygen and with sulfur hexafluoride were measured in hydrothermal and supercritical water using transient absorption spectroscopy and electron pulse radiolysis. Under alkaline conditions, the reaction of hydrogen atoms with hydroxide ions to generate solvated electrons was also observed in the presence of the SF_6 scavenger. At temperatures below 300 °C, the rate constants for scavenging by O_2 or SF_6 follow Arrhenius behavior but become increasingly dependent on water density (pressure) at higher temperatures. Above 100 °C, the rate constant for the H reaction with OH^- falls well below the numbers extrapolated from the Arrhenius behavior in the one atmosphere liquid. At a fixed temperature above the water critical temperature (380 °C, $T/T_c=1.01$), rate constants for all three reactions reach a distinct minimum near 0.45 g/cm^3. We propose an explanation for this behavior in terms of the potential of mean force separating an ion (OH^- or $(e\text{-})_{aq}$) from a hydrophobic species (H, O_2, or SF_6) in the compressible fluid. The data also reveal an increasing initial yield of atomic hydrogen relative to solvated electrons as water density decreases. The initial yield of H appears to surpass that of solvated electrons when the water density is below 0.6 g/cm^3 at 380 °C.

I. Introduction

Commercial nuclear reactors provide a source of heat, used to drive a "heat engine" (steam turbine) to create electricity. A fundamental result of thermodynamics shows that the higher the temperature at which any heat engine is operated, the greater its efficiency. Consequently, one obvious way to increase the operating efficiency for future nuclear power plants is to heat the water of the primary cooling loop to higher temperatures. Current pressurized water reactors run at roughly 300 °C and 100 atm pressure. Designs under consideration would operate at 450 °C and 250 atm, i.e., well above the critical point of water.[1−3] This improves the attainable efficiency by about 30% and is successfully used in many conventionally fired power plants. In the context of nuclear power, however, a major unanswered question is what changes occur in the radiation-induced chemistry in water as the temperature and pressure are raised beyond the critical point and what this could imply for the limiting corrosion processes[3−5] in the materials of the primary cooling loop. This manuscript represents the first in a series that will attempt to provide fundamental data (yields and reaction rates) to answer this question.

Quite apart from the practical motivation for this project, the study of free radical reactions in the supercritical water regime is interesting in light of recent work on reaction rate theory and spectroscopy in compressible supercritical fluids.[6−15] The primary free radicals generated by radiolysis, $(e^-)_{aq}$, OH, and H, are respectively ionic, dipolar, and hydrophobic in nature. Their recombination and scavenging reactions can be expected to highlight the effects of clustering (i.e., local density enhancements) both in terms of relative diffusion and static or dynamic solvent effects on the reaction rates. The temperature and pressure effect on the solvated electron spectrum is another subject of fundamental interest which will be addressed in a future paper.[16]

The radiolysis of water by neutrons, recoil ions, gamma photons, and high-energy electrons can be represented by

$$H_2O \xrightarrow{\text{radiation}} (e^-)_{aq}, H^+, H, H_2, OH, H_2O_2, HO_2 \text{ (or } O_2^-) \quad (1)$$

Energy tends to be deposited in isolated spurs and tracks so that recombination of the reactive transients occurs on a nanosecond time scale in competition with diffusive escape.[17−22] A chemical reaction of critical importance in nuclear-reactor coolant is the reaction of the hydroxyl radical with hydrogen to produce hydrogen atoms and water:

$$OH + H_2 \rightarrow H + H_2O \quad (2)$$

This is the only reaction that can occur sufficiently quickly to convert the oxidizing radical, OH, into the reducing radical, H, before OH reacts in an oxidizing reaction. The reaction of OH as an oxidizing radical must be prevented to suppress oxidative corrosion in the primary heat transport system. When a sufficient quantity of excess hydrogen gas has been added to the reactor coolant, the net production of oxygen and hydrogen peroxide becomes essentially zero.[4,23] Other reactions

† Work performed under the auspices of the Office of Science, Division of Chemical Science, US-DOE under Contract No. W-31-109-ENG-38. Additional funding was provided under Nuclear Energy Research Initiative Grant No. M9SF99-0276.

* To whom correspondence should be addressed.

‡ Permanent address: Division of Quantum Energy Engineering, Hokkaido University, Sapporo 060-8628, Japan.

10.1021/jp0270250 CCC: $22.00
Published on Web 12/03/2002

occurring include the following:[17,24]

$$OH + OH \rightarrow H_2O_2 \quad (3)$$

$$(e^-)_{aq} + (e^-)_{aq} \rightarrow 2OH^- + H_2 \quad (4)$$

$$OH + O_2^- \text{ (or } HO_2) \rightarrow OH^- + O_2 \quad (5)$$

$$(e^-)_{aq} + OH \rightarrow OH^- \quad (6)$$

$$(e^-)_{aq} + H_2O_2 \rightarrow OH + OH^- \quad (7)$$

$$(e^-)_{aq} + H^+ \rightarrow H \quad (8)$$

$$(e^-)_{aq} + H \rightarrow H_2 + OH^- \quad (9)$$

$$H + H_2O_2 \rightarrow OH + H_2O \quad (10)$$

$$(e^-)_{aq} + O_2 \rightarrow O_2^- \quad (11)$$

and at alkaline pH

$$H + OH^- \rightarrow (e^-)_{aq} \quad (12)$$

Basically, all of the species in (1) can react with each other, but some reactions are much more important (faster) than others. Reaction 2 is the overall rate-determining reaction in the production of oxygen or peroxide. Reactions 2 and 10, or 2, 12, and 7, constitute chain reactions that can consume hydrogen peroxide, which prevents significant formation of O_2^-, H_2O_2, and O_2, in quantities that could otherwise exacerbate degradation of materials in the heat transport system.

Direct measurement of the chemistry in reactor cores is extremely difficult, if not impossible. The extreme conditions of high temperature, pressure, and radiation fields are not compatible with normal chemical instrumentation. There are also problems of access to fuel channels in the reactor core. For these reasons, theoretical calculations and chemical models have been used extensively, by all reactor vendors and many operators, to model the detailed radiation chemistry of the water in the core and the consequences for materials. Data required to model this chemistry up to 300 °C (the operating temperature of pressurized water reactors or PWRs) have been collected and summarized by Elliot and co-workers at AECL for both light[24] and heavy water.[25] For many of the dominant reactions, data have been measured up to 200 or 250 °C, and some measurements have been taken to 300 °C, but significant gaps in the database remain. In particular, the recombination reaction 4 of two solvated electrons shows a very strange temperature dependence above 150 °C that has not been explained.[25,26] Reaction 12 has only been measured up to 95 °C,[27,28] and we will show in this study that one cannot extrapolate to higher temperatures using a simple Arrhenius expression.

In the following sections, we study directly the reactions of solvated electrons with scavengers O_2 and SF_6. The intense visible absorption of the solvated electron is very easy to measure in a pulse radiolysis/transient absorption experiment. Oxygen is both easy to add to water and must be removed for other experiments, so we begin our studies with an investigation of the temperature and pressure dependence of reaction 11. The reaction with SF_6 was chosen on a more practical ground.

To extract second-order reaction rate coefficients, it is necessary to determine absolute extinction coefficients for some species under supercritical conditions. Our plan has been to use

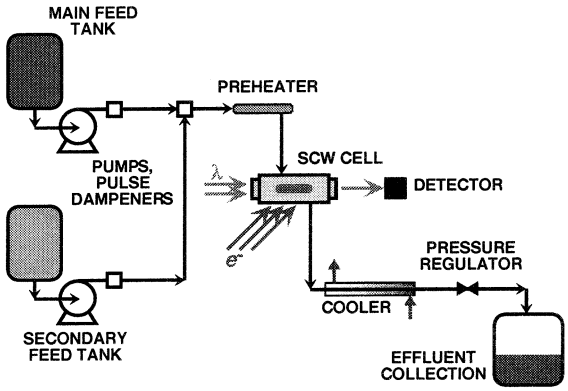

Figure 1. Experimental configuration for supercritical water radiolysis transient absorption.

SF_6 as a scavenger for solvated electrons and directly measure both the transient absorption and resulting chemical product. In aqueous solution, SF_6 is chemically inert and highly stable over wide ranges of temperature,[29] except in the presence of solvated electrons,[30]

$$(e^-)_{aq} + SF_6 \rightarrow F^- + SF_5 \quad (13a)$$

$$SF_5 + 4H_2O \rightarrow SO_3^= + 5F^- + 7H^+ + OH \quad (13b)$$

This selective stability makes it a suitable scavenger for solvated electrons in the aggressive environment of supercritical water. The stable ionic products can be measured by conductivity and ion chromatography in line with the radiolysis flow cell.

We measured the reaction rates of solvated electrons with SF_6 over a range of temperature and pressure conditions and in the presence of hydroxide to neutralize the acid product. To our surprise, reaction 12 was immediately visible as a second exponential tail on the electron decay kinetics, because the relative initial yield of H atoms in supercritical water is much higher than in ambient conditions. In this paper, we therefore report reaction rates for reactions 11−13 as a function of water temperature and density, as well as relative initial yields of H and $(e^-)_{aq}$.

II. Experimental Section

The experiment is shown in schematic form in Figure 1. The kinetics of solvated electrons were measured by pulse radiolysis and transient absorption spectroscopy in a special high-pressure, high-temperature flow cell described previously.[31] The optical windows are sapphire, and the cell body is Hastelloy C-276 alloy.

At the cell, solvated electrons (and other transient species) were generated using 4 and 8 ns pulses from Argonne Chemistry Division's 20 MeV electron linac. The dose to water was 15−20 Gy per 30 ps or 4 ns pulse; pulse amplitude was constant to 5% or better during a daylong experiment but varied between days. Because of the difficulty with all-metal connections to the cell, the charge per pulse was not measured for relative dosimetry.

The analyzing light was generated by a focused 75 watt xenon-arc lamp, which was pulsed for approximately 300 μs, timed such that the linac pulse coincided with the flattest part of the lamp pulse. Wavelength selection was achieved using 40 nm bandwidth interference filters. The choice of wavelength varied with water temperature and density. At higher temperatures and lower densities, the solvated electron spectrum is red-shifted.[26,32,33] In general, for most elevated-temperature

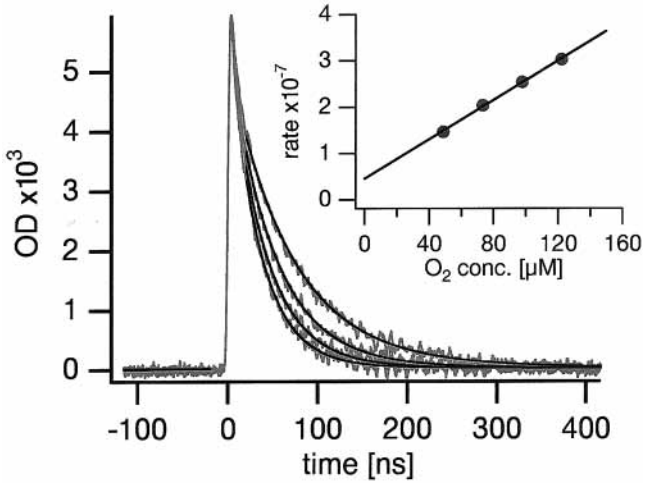

Figure 2. Sample fitted data and pseudo-first-order plot for scavenging of solvated electrons by O_2. The conditions were 370 °C and 204 bar, in the subcritical vapor phase (0.165 g/cm^3).

conditions, we used 1000 nm; the kinetics at 200 °C and below was measured at 700 nm.

Transmitted light was measured using an EG&G FND100Q silicon photodiode for 700 nm light and a Germanium Power Devices GAP520 InGaAs diode for 1000 nm light. Diode photocurrents during the lamp pulse were typically in the 5−50 mA range. The signal was acquired using a Tektronix TVS645A digital waveform analyzer (1 GHz bandwidth, 5 GHz sampling) controlled via GPIB through extensions to Wavemetrics' IGOR program. Data were taken using a 250 MHz bandwidth filter (1.2 ns rise time). The DC offset and gain were routinely adjusted to use most of the 8-bit resolution for the transient signals. For most conditions, averaging six trace "sets" was more than sufficient to provide a clear signal down to the 10^{-3} OD level (see Figure 2), where each "set" consists of a signal trace minus a dark trace (closed shutter) to subtract RF noise from the linac. For short acquisitions ($\leq$1.6 μs), the baseline light was assumed to change linearly with time; for longer intervals, the full baseline lamp shape was recorded and used to compute OD(t).

The GAP520 InGaAs diode was found to have a secondary response that distorts the kinetic measurements on a one-microsecond time scale. (A secondary response is also found in the FND100 silicon diode for wavelengths longer than 800 nm.) For pure first-order kinetics, this requires a relatively minor correction, but it becomes more important in the analysis of biexponential kinetics. Measurements from the GAP520 at 1000 nm were compared with reliable measurements from time-correlated absorption experiments and measurements with an FND100Q photodiode at a state point (45 °C, 1 bar) where the solvated electron spectrum is stable and well-known, and the spur kinetics are well-characterized down to a picosecond time scale.[34] Comparison of transmission curves allowed generation of an approximate impulse response function (a delta function and an exponential decay).[35] The GAP520 has a secondary response with a time constant of approximately 800 ns, whose integral amounts to 10% of the integrated current signal. During curve fitting, each model curve was convolved with this instrument response before comparison to the experimental data.

Two water reservoirs, sparged at atmospheric pressure with Ar and O_2 or SF_6, respectively, fed two independent Alltech HPLC pumps. As described in Takahashi et al.,[31] extra HPLC pulse dampeners were connected to each pump outlet, to ensure smooth flow. Both flow streams proceeded to a mixing tee and then through a preheater to the optical cell. From the cell, flow proceeded through a water-cooled shell-and-tube heat exchanger, where it was cooled to room temperature. Pressure let-down was effected using either a back-pressure regulator or a length of PEEK plastic or stainless steel capillary tubing (see Figure 1). System pressure was monitored at the exit of the cool-down heat exchanger using a high-sensitivity piezoelectric transducer of 2.5 psig calibrated accuracy (Omega PX02 series). Temperature was monitored using thermocouples immersed in the flow at the exit of the preheater and within the cell. Overall system stability was roughly $\pm$0.5 °C, and $\pm$1 bar for supercritical conditions.

Scavenger concentration was modified by changing the ratio of the flow rates of the feed pumps. The concentrations of SF_6 and O_2 in the water were computed using the equilibrium data of Cosgrove and Walkley[36] with the flow fraction of the scavenger-saturated stream and the fluid density as computed from the NBS Equation of State.[37] Flow rate was kept constant for any given state point at values ranging from 2.5 to 6.0 mL/min; these low, constant flow rates ensured that (a) the system was isobaric and (b) the temperature in the flow cell was constant, whereas (c) radiolysis products were not allowed to accumulate in the once-through flow cell. (No more than three or four beam pulses could irradiate the cell in the flushing time, which is insufficient to affect the pseudo-first-order kinetics under study.) In general, flows of 6 mL/min were used when the back-pressure regulator was in place; for capillary tubing, the flow rate was 2.5−4.0 mL/min as required to set the pressure.

Ar-sparged, ultrapure (18 MΩ-cm) water flowed through one pump during system heat-up. A second pump head was primed to feed SF_6- or O_2-saturated water. For SF_6 experiments employing alkaline conditions, after heat-up, the feed was switched to Ar- and SF_6-sparged potassium hydroxide solutions. Special care was taken to reduce or eliminate O_2 and CO_2 contamination of the solutions. Precautions against O_2 contamination were particularly important for alkaline-solution experiments, as it seemed that if any trace of residual oxygen remained in the system when switching to alkaline feeds, the sapphire windows were etched, dramatically reducing the transmitted light.

At each P−T state point, the scavenger concentration was set initially low and then increased. This precaution was taken because we found that the system plumbing could act as a scavenger reservoir. For example, although responses to increasing flow of SF_6-saturated water were immediate, we found it could take up to an hour after shutting off the SF_6-saturated water to flush it all out, as determined from observation of the solvated electron lifetime; a similar but much less dramatic effect was seen with oxygen (i.e., the flush out was several times faster). In contrast, salt solutions were readily flushed through within a minute. Because the system was always at pressures $\geq$100 bar, at no time were the gas solubilities expected to fall below the molal saturation concentration for 1.0 atm at 25 °C. Additionally, the use of zero-dead-volume HPLC fittings eliminated the possibility of a vapor reservoir developing in the upstream system; there was no second phase visible in the optical cell.

Eventually, it was realized that actual concentrations of SF_6 in the irradiation cell were not as high as expected (see below) and that the discrepancy became more severe as the flow rate of the SF_6-saturated water decreased. SF_6 delivery to the cell was tested by collecting water from various points in the flow system in a glass syringe. The syringe was irradiated to convert

all SF_6 to fluoride and sulfite via reaction 13. Then the fluoride concentration was measured with ion chromatography. This diagnostic showed that SF_6 was being stored in or lost through the oxygen-impermeable plastic tubing used between the reservoir and pump and also in the HPLC pulse dampeners whose construction includes a plastic diaphragm. All stainless steel tubing and a different dampener arrangement have since resolved the problem. Although we make a correction for this concentration problem, the SF_6 rate constants presented below are somewhat more approximate than the other numbers we report. We should emphasize that the SF_6 itself is entirely stable under the supercritical water conditions we have explored. No conductivity change in the (nearly 18Mohm-cm) neutral water effluent could ever be detected to indicate a thermal breakdown of the SF_6 to hydrofluoric acid and sulfite. No similar retention for oxygen was found.

Most of the SF_6 scavenging experiments described below were performed in the presence of 0.5 or 1.0 millimolal KOH. Addition of the electrolyte to the solution raised concerns of whether density changes due to electrostriction would be significant and also whether the KOH was fully dissociated. No partial molal volume data could be found for KOH or NaOH at 380 °C and 250 bar, to address the electrostriction issue. The literature does show that, in supercritical water, OH^- behaves volumetrically as Cl^-;[38] we thus examined the behavior of NaCl to estimate behavior of KOH. In the work of Majer and Wood,[39] we find that at 280 bar and 378 °C the infinite-dilution partial molar volume of NaCl is -1059 cm^3 mol^{-1}, which for molalities of 10^{-3} produce only a change in volume of -0.05% at 280 bar and 378 °C. Although it cannot be ruled out that at lower densities the effect will become stronger, it must increase by two orders of magnitude to influence our results significantly.

The degree of dissociation is estimated after the approach of Ho et al.[38] Using the extended form of the Debye−Hückel limiting law, and assuming a continuum dielectric fluid, we estimate an activity coefficient of approximately 0.79, which results in a degree of dissociation within 0.1% of unity at 0.5 g/cc. The available data extend only to 0.4 g/cc, and at lower densities, we might expect some association to affect rate constant k_{12}. Our available data for two KOH concentrations (1.0 and 0.5 molal) show no effect on k_{12} for the range of densities studied (greater than 0.1 g/cm^3).

III. Results and Analysis

Oxygen. An extensive survey of solvated electron scavenging by oxygen (reaction 11) was carried out for different *T*, *P* conditions in the water critical region. All of the fitted rate constants, with estimated errors (one standard deviation) are listed in Table 1S of the Supporting Information. A typical data set is illustrated in Figure 2, for scavenging at 370 °C and 204 bar in the high-density vapor phase (density 0.158 g/cm^3). The GAP 520 diode was used at 1000 nm for detection. The fitted curves shown include the small correction for secondary diode response mentioned above. In general, the fitting was started from approximately 20 ns after the pulse to avoid distortions from linac noise and from spur recombination chemistry.

Results for the measurements at 250 bar and some lower pressures are plotted in the Arrhenius format in Figure 3. Below 300 °C the reaction rate is very insensitive to the pressure. The Arrhenius curve adapted from the compilation of Elliot[24] from room temperature to 200 °C is also superimposed for comparison. Clearly, the agreement of our measurements with previous work is quite good. Along the 250 bar isobar, a strong dip in reaction rate is visible in the critical region, with a minimum at 380 °C.

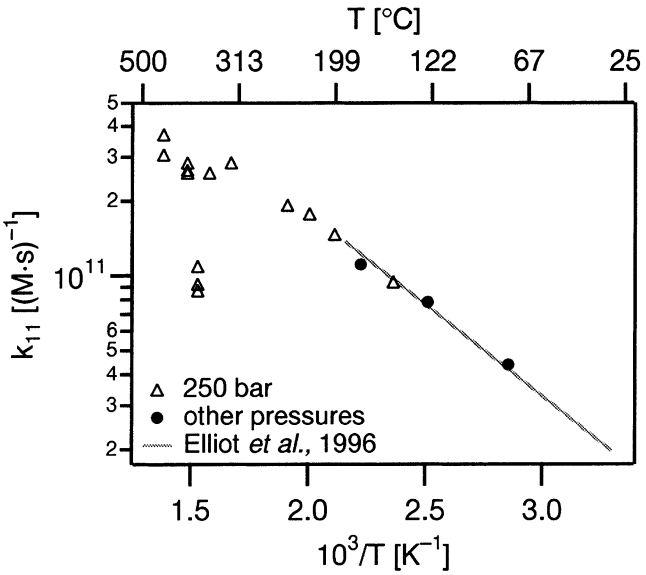

Figure 3. Arrhenius plot of reaction 11 at 250 bar and lower pressures, compared to existing literature.[25] The rapid dip in rate at 380 °C illustrates the effect of the compressible solvent on the reaction rate.

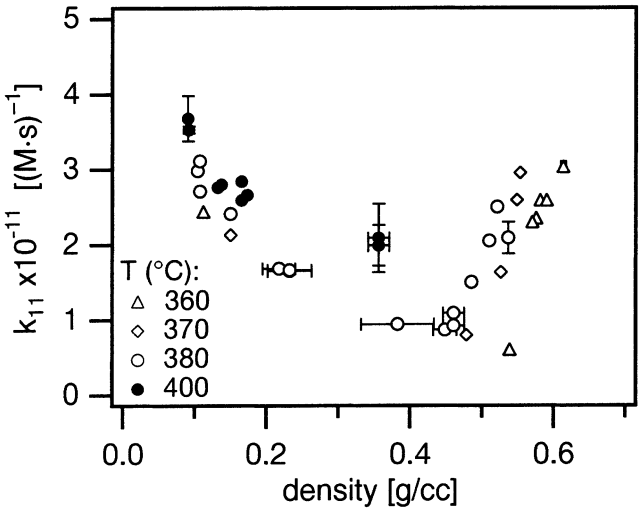

Figure 4. Effect of density on rate constant of reaction 11 at various near-critical temperatures. Except where shown explicitly, the errors are on the order of the symbol size.

The phase-point behavior is more clearly represented in Figure 4, where we plot rate constants for 360, 370, 380, and 400 °C as a function of the water density. The error bars depend strongly on the density as indicated because in the compressible region it is more difficult to maintain constant temperature and pressure. A very sharp drop in the rate constant is obvious as we proceed from high density down to about 0.45 g/cm^3 on a given isotherm. Proceeding along the 380 °C isotherm, the rate increases again down to the lowest densities measured. Although the intermediate densities are not available for the subcritical isotherms at 360 and 370 °C, the dense vapor (0.10−0.16 g/cm^3) at these temperatures shows the same behavior as the supercritical 380 °C reaction rate. The isochoric activation energy on this low-density side is apparently quite small. The high-density side is not available at 400 °C because the large pressures required exceed the capabilities of the pumps. The rate constants in the compressible region around 0.3 g/cm^3 are significantly higher at 400 °C than at 380 °C, and the overall effect of density is less at the higher temperature.

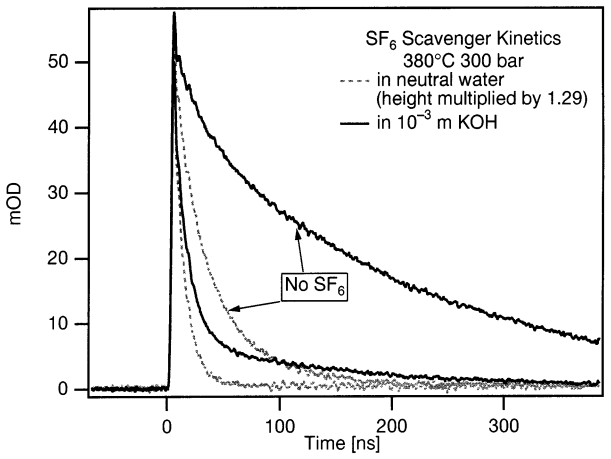

Figure 5. Effect of KOH on decay rate of solvated electrons in supercritical water (380 °C, 300 bar, 0.534 g/cc). In the presence of 1.2×10^{-4} M SF_6 scavenger, the long tail on the kinetics in alkaline solution is due to conversion of H atoms to solvated electrons.

The error bars in Figure 4 correspond to the error from the curve fit as well as uncertainties in density. The majority of the error stems from uncertainties in the temperature and pressure coupled with large isothermal compressibilities. For instance, the error propagation from measurements P and T to density is computed through thermodynamic properties:

$$\sigma_\rho^2 = (\kappa_T/V)^2[\sigma_P^2 + (\partial P/\partial T)_V^2 \sigma_T^2] \qquad (14)$$

where κ_T is the isothermal compressibility of the fluid, and the σ_i's are the estimated standard errors of the measured quantities. The error bars extend to a width of 2σ (i.e., the interval is mean-(x) $\pm$ σ). Because of increasing fluctuations near the critical density ($\rho = 0.32$ g cm^{-3}) and finite instrument response time, the magnitude of the errors may be systematically underestimated at these points.

SF_6. As explained in the Introduction, we measured the scavenging of SF_6 in alkaline solution to avoid any problems with buildup of hydrofluoric acid product. Figure 5 compares the kinetics observed in neutral and alkaline solution at 380 °C and 300 bar (0.534 g/cm^3). In the absence of SF_6, the electron absorption decays to baseline within 200 ns in neutral solution but lasts nearly a microsecond in 10^{-3} molal KOH solution. This comparison clearly illustrates the importance of reaction 8 in the electron decay under these conditions.[40] Addition of 1.2×10^{-4} molar SF_6 causes the electron to decay to the baseline within about 50 ns in neutral solution. In 1.0 millimolal KOH solution, the solvated electron concentration quickly decays to approximately 10% of its initial value and then persists with a dramatically slowed decay.

Figure 6 illustrates the qualitative behavior of the scavenging kinetics in alkaline solution above 300 °C. Within a few nanoseconds after the pulse (some spur decay is apparent), the decays are biexponential. Addition of SF_6 scavenger shortens the initial (fast) decay time and reduces the amplitude of the signal at long time. The time constant for the slow decay is unaffected. Under alkaline conditions, reaction 12

$$H + OH^- \rightarrow (e^-)_{aq} + H_2O \qquad (12)$$

acts as a secondary source of solvated electrons. This source becomes dominant after the scavenger has depleted most of the initial $(e^-)_{aq}$ and the residual absorption is the result of competition between source and sink. Because reaction 12 is much slower than the reaction of the electron with SF_6, the slow

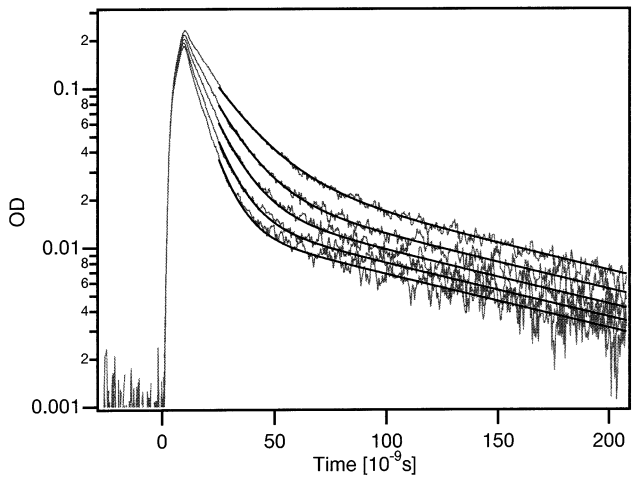

Figure 6. Log plot of data for reactions of solvated electrons and SF_6 in alkaline water at 350 °C and 304 bar (0.646 g/cc) following 8 ns electron pulses ([KOH] = 10^{-3} mol kg^{-1}; [SF_6] = 1.6×10^{-4}–2.5×10^{-4} mol L^{-1}).

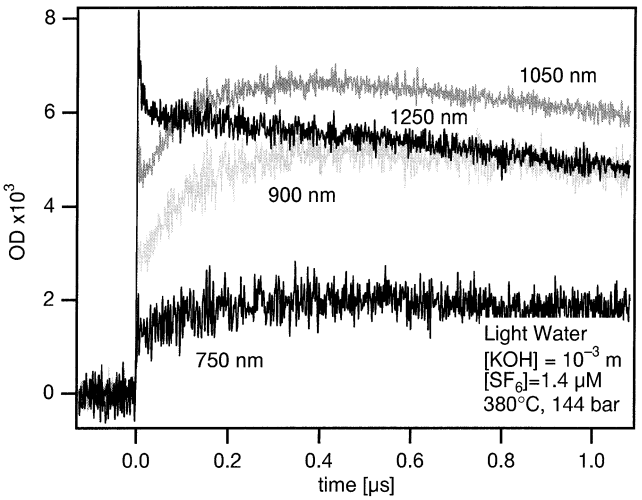

Figure 7. Transient spectral shift of $(e^-)_{aq}$ in alkaline water vapor (380 °C, 144 bar, 0.066 g/cc). A pure decay is seen at 1250 nm, but at shorter wavelengths, first a rise and then a decay is seen.

decay directly gives the rate of reaction 12. The rate of this reaction depends on the concentration of OH^- and is independent of the concentration of SF_6, as can be seen in Figure 6. The relative magnitude of the slowly decaying component increases at lower water densities. This shows that the initial yield of H atoms increases relative to the yield of (e-)$_{aq}$, as will be discussed below.

At very low densities at 380 °C, we discovered a dynamic shift of the solvated electron spectrum that made the apparent decay rate at 1000 nm slower. In Figure 7, it is clear that at 144 bar (0.066 g/cc) the spectrum of the solvated electron shifts dynamically to the blue in the first 200 ns after the electron pulse. This effect disappears at pressures above 190 bar (0.107 g/cm^3). We assume the spectral shift is due to ion pairing of the electron with counterions; a detailed analysis will be published in the future. Because of the severity of the effect, short-time scale data at pressures 190 bar and below (at 380 °C) have been excluded from the present analysis of alkaline solutions.

Preliminary analyses fitted the data at a given dose and SF_6 concentration assuming a biexponential form. The slow component of the biexponential decay appears to be independent of dose. The fast component of the biexponential decays in

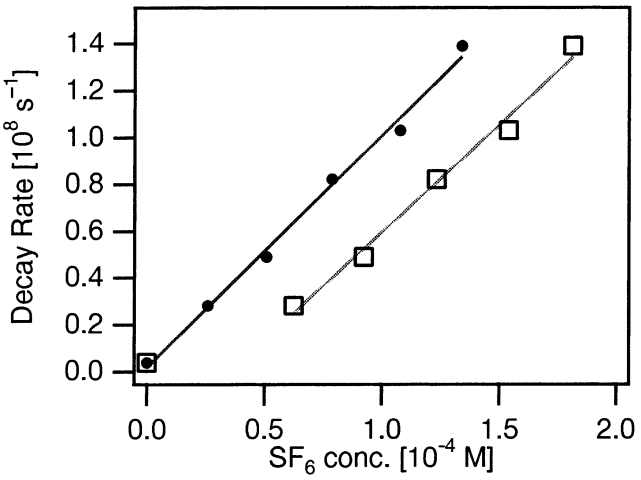

Figure 8. Nominal (squares) and corrected SF_6 concentration (circles) pseudo-first-order plots for reaction 13. These data correspond to 300 °C at 252 bar.

Figure 6 should represent the desired reaction of $(e^-)_{aq}$ with SF_6. As shown in Figure 8, typical pseudo-first-order kinetics were seen for this component, except that a negative intercept was often found and that the intercept depended on dose. We determined (only after collection of all of the kinetics data reported here) that much SF_6 was lost by diffusion into plastic elements of the flow system before it reached the all-metal preheater and cell (see the experimental description above). For corrections, the final SF_6 concentrations used for the fits described below were estimated using a steady-state mass transfer equation:

$$[SF_6]_{real} = [SF_6]_{nom} \exp(-H_0Ax/q_{SF6}) \qquad (15)$$

where (H_0Ax) is an overall mass transfer coefficient and q_{SF6} is the volumetric flow rate of saturated solution through the tube. A corrected scavenging line is illustrated in Figure 8. The lower nominal concentrations correspond to lower flow rate of the SF_6-saturated water feed and longer contact time between the SF_6 and plastic elements of the flow system. Note that at the lowest flow rate, 50% of the SF_6 was lost before it reached the cell. On the other hand, the highest flow rates were only slightly affected.

The rate constants k_{12}, k_{13}, and the "initial" ratio G_H/G_e of H and $(e^-)_{aq}$ yields were evaluated from the experimental data by simultaneously fitting the experimental decays for a sequence of concentrations and radiation doses acquired on a given day. As mentioned above, the slow component is independent of dose except in the limit of low SF_6 concentration, which suggests that second order reaction of the H atoms with other H and OH radicals can be largely ignored. The dose dependence in fitted G_H/G_e must be dominated by second-order reactions of $(e^-)_{aq}$ with H (reaction 9) or possibly OH (reaction 6) at early times. (We note that reaction 6 has a relatively low activation energy where it is measured below 200 °C.) To correct for the dose dependence, we include the second-order rate constant k_9 as a fitting parameter, assuming a constant extinction coefficient of 10 000 M^{-1} cm^{-1}. (This assumption will affect the value of k_9 but will not affect the values for k_{12}, k_{13}, and G_H/G_e.) The numbers for k_9 are included in the results Table S2 for completeness but should not be considered quantitatively accurate. The value of k_9 reported will include other second-order reactions and reactions of impurities that might be present.

The appropriate differential equations for the system of reactions 9, 12, and 13 were integrated using a stiff differential equation integrator. The least-squares fitting used a conventional Levenberg−Newton minimization. Data were fitted starting after effects of nonhomogeneous kinetics and cable ringing had died away (less than 20 ns after the pulse) The shape and length of the irradiation pulse were included in the integration of the equations as were the response characteristics of the detector. Data were fitted either by optimizing the value of H_0Ax or by setting the value of H_0Ax to zero and using only the higher SF_6 concentrations (flow rates). All of the 380 °C data are reported with $H_0Ax = 0$ to give the maximum consistency for plots vs density. The data shown in Figure 10 are thus a lower limit to the true rate constant. As shown in Table 2S when both analyses were done on the same data sets, the differences in the rate constant were less than 30%. Results for k_{12} and for G_H/G_e are unaffected by the uncertainty in SF_6 concentrations.

Possible errors in k_{12}, k_{13}, and G_H/G_e were evaluated both by considering the covariance matrix and by probing the curvature of the chi-square surface by perturbing a fitted constant and refitting the data. Except for k_{12}, the fitted constants are constrained to within 10% for all conditions, excluding the role of H_0Ax discussed above. Typical errors for k_{12} are included in Figure 11; the uncertainty is much larger than 10% below 250 °C because G_H/G_e becomes quite small, and there is little signal

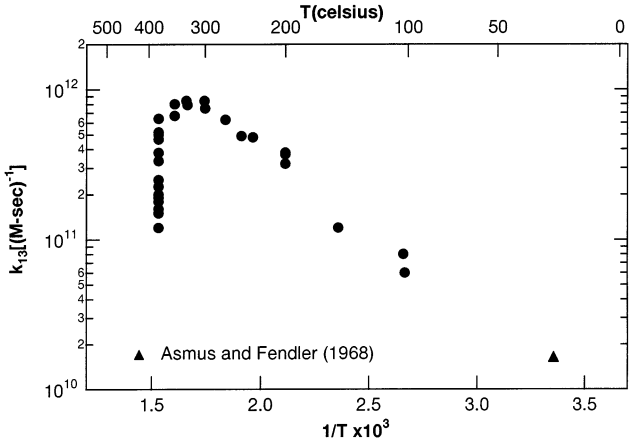

Figure 9. Arrhenius plot for reaction 13. Errors in the experimental rate constants are approximately 10%. The leftmost data are for 380 °C at various pressures. At lower temperatures, the water pressure was typically between 200 and 300 bar. Below 350 °C, the pressure has little effect on the density or the reaction rates.

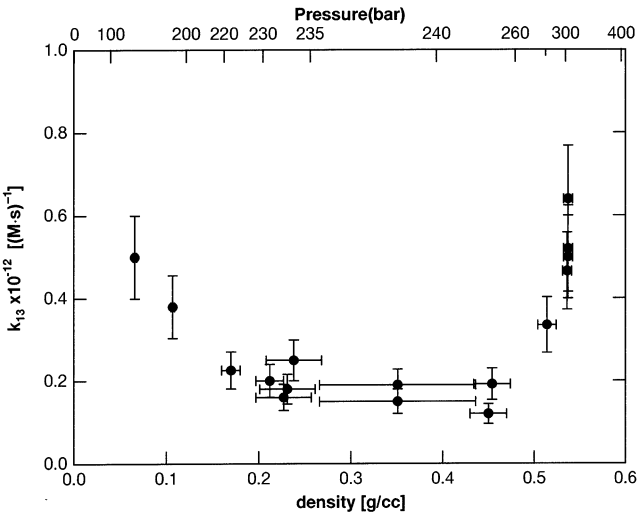

Figure 10. Effect of density on rate constant for reaction 13 at 380 °C. Error in these rate constants may be 50% due to uncertainties in the SF_6 concentrations (see text).

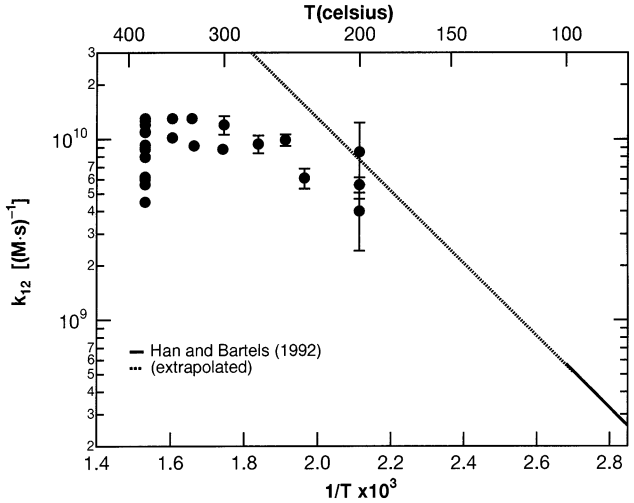

Figure 11. Arrhenius plot for reaction 12 at various pressures. The errors in the rate constants are approximately 10%. The leftmost data are for 380 °C. The straight line is from reference 28.

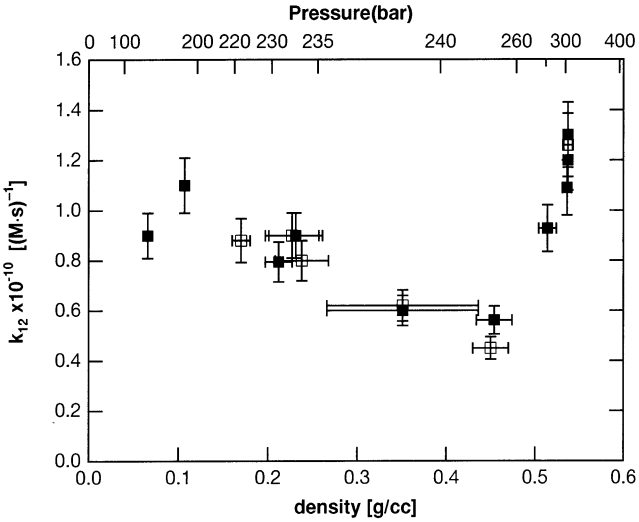

Figure 12. Effect of density on apparent rate constant for reaction 12 at 380 °C. The filled and open symbols represent KOH molalities of 1.0×10^{-3} and 0.5×10^{-3} mol kg^{-1}, respectively.

to fit. It was not possible to use the covariance matrix results directly because the error surface is not quadratic over a sufficiently large range.

Figure 9 shows an Arrhenius plot of the second-order rate constant for scavenging of electrons by SF_6. Our new measurements nicely connect to the room-temperature result of Asmus et al.[41] The simple Arrhenius behavior is followed until the fluid becomes relatively compressible. Above 350 °C ($1000/T = 1.6$), the density becomes extremely important. The column of points at the high-temperature side of the plot corresponds to 380 °C and various pressures/densities. Figure 10 shows these data as a function of density. The behavior is similar to the observations for O_2 scavenging shown in Figure 3.

Figures 11 and 12 show similar behavior in the reaction of OH^- with H atoms. A nearly identical result has been obtained by Percival and co-workers for the reaction of muonium (a light isotope of atomic hydrogen formed with a positive muon as nucleus) with OH^- in supercritical water.[42] The new rate constants connect to the high-precision data of Han and Bartels[27,28] (Figure 11), but the Arrhenius activation energy becomes smaller above 100 °C. Earlier models that extrapolated the Han and Bartels result to high temperature are seen to be

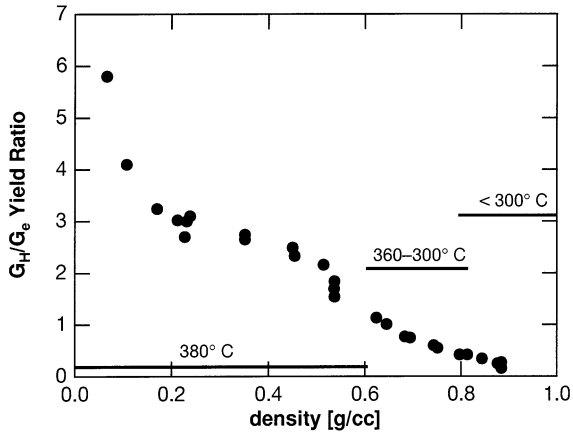

Figure 13. Change of apparent yield ratio G_H/G_e with solution density. Above $\rho = 0.6$, density is chiefly governed by temperature.

unjustified.[24,25,43] The character of the density dependence at 380 °C is virtually the same as for reactions 11 and 13, though the rate constants for reaction 12 are an order of magnitude smaller.

Figure 13 displays the ratio of initial yields for H atom and solvated electron. Up to this point we have made no attempt to establish absolute yields. The ratio G_H/G_e is small (ca. 0.25) at high density and temperatures below 250 °C, in agreement with previous studies of gamma radiolysis.[24] Above this temperature, for densities in the range of 0.6−0.75 g/cm^3, the ratio increases. At 350 °C, the ratio is approximately 1.0. In supercritical water at 380 °C, the measured G_H/G_e ratio is greater than unity and becomes larger as density decreases. In low-density supercritical water, the initial yield of H atoms seems to be roughly five to six times the yield of hydrated electrons.

Where experiments were performed at two different OH concentrations for the same state point, results for k_{12} were found to be within l0%. The graphs for reaction 13 lack vertical error bars because of uncertainty in the amount of SF_6 delivered to the cell as discussed above. (A conservative upper limit on the uncertainty is a factor of 2.)

IV. Discussion

Two striking and unexpected observations come out of this study. The first is the strong decrease and then increase of the rates for reactions 11−13 as a function of density in supercritical water at 380 °C. The second is the apparent increase in H atom yield, relative to solvated electrons, as density decreases and temperature increases above 300 °C.

With regard to the rate constants, the first question to settle is whether the behavior results from a diffusion limit or from an activation barrier. The reaction of solvated electrons with O_2 up to 100 °C was considered in a previous study in this laboratory.[44] It was shown based on the measured diffusion coefficients that the reaction must be a diffusion-limited long-range electron transfer over most of this temperature range. However, the average Smoluchowski reaction distance decreases with increasing temperature from 7 Å near room temperature to 3 Å at 100 °C. Because the activation energy of the reaction (14.0 kJ/mol) is well below the activation energy for electron diffusion (20.2 kJ/mol),[44] reaction 11 is certainly not diffusion-limited at higher temperatures. For reaction 13, the room-temperature rate constant of 1.6×10^{10} M^{-1} s^{-1} is very high but still smaller than diffusion limited. An estimate of the diffusion-limited rate based on the Smoluchowski equation,[45] with a relative diffusion coefficient of 6.0×10^{-5} cm^2 s^{-1} and

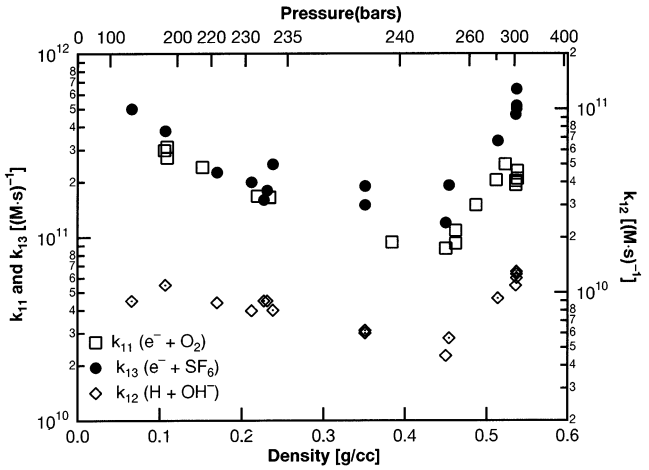

Figure 14. Density dependence of three reactions at 380 °C. Note the log scale for k_{12} (right side) is shifted for easy comparison with the other reactions.

reaction distance of 6.0 angstroms, is 2.7×10^{10} M^{-1} s^{-1}. At 150 °C, we measure a rate constant of 1.9×10^{11} M^{-1} s^{-1}, and the Smoluchowski equation predicts 5.1×10^{11} $M^{-1}s^{-1}$. (Again the relatively large activation energy for solvated electron diffusion dominates.[44]) Thus, reaction 13 is also further away from pure diffusion control at elevated temperature. Indeed, it has proven difficult to find purely diffusion-limited reactions over a wide temperature range in water. More often than not, a small activation barrier limits the rate at elevated temperatures.[46]

We have no data on diffusion coefficients for the solvated electron above 150 °C, so we cannot completely rule out partial diffusion-limited behavior for reactions 11 and 13 at 380 °C. Between 300 and 600 °C, the conductance of simple 1:1 electrolytes shows no dramatic change in the density range around 0.4−0.6 g/cm^3, suggesting that ionic diffusion is not responsible for the unusual reaction rate behavior.[47] Most importantly, reaction 12 is very far from the diffusion limit at lower temperatures and is still an order of magnitude slower than reactions 11 and 13 at 380 °C. In Figure 14, we show that the rate constants of reactions 11−13 can be virtually superimposed merely with a constant multiplier. This strongly suggests that the entire density effect on the rate constants is unrelated to diffusion.

It may be instructive to consider just how different these reactions are. As we noted above, the reaction of solvated electron with O_2 is best thought of in terms of an electron transfer from a potential minimum formed by the solvent molecules, into a potential minimum centered on the oxygen molecule.[44] In principle, the Marcus theory of electron transfer rates should apply. The same picture should apply to the reaction of electrons with SF_6, but in this case, the product immediately dissociates into SF_5 and F^-. In either case, the reaction (whether diffusion-limited or not) may occur by electron transfer from "long range" without direct "contact" between the electron and scavenger. In contrast, the reaction of H atoms with OH^- is best thought of as a "proton transfer", in which the electron is "left behind" in the solvation cavity originally occupied by the H atom.[28] Immediate contact between H and OH^- is probably necessary to effect the proton transfer. The activation energy is relatively high, and the reaction rate is well below the diffusion limit. The only common feature of all of these reactions is that they each involve a hydrophobic species and a solvated anion. We surmise that the explanation is found in consideration of the potential of mean force separating the hydrophobic and ionic species in the compressible fluid.

The nature of solvent clustering and local density enhancements in supercritical fluid has been much discussed in the recent literature.[48,49] The picture that emerges is that, near the critical region, the entropic driving force that favors vaporization roughly balances the attractive potential between solvent molecules responsible for condensation. Microclusters of molecules are constantly forming and dissipating. In this environment, a solute molecule with attractive potential relative to the solvent will tend to form the nucleus of a cluster and be found in a region of local density enhancement relative to the bulk average. A solute with repulsive potential can expect to be found more often in the voids between the dynamic solvent clusters.[50]

Evidence for these effects in water can be found in the large negative partial molal volumes of ions (attractive potential) and large positive partial molal volumes of hydrophobic (repulsive potential) molecules and atoms.[48] Biggerstaff and Wood[51] note that, for argon, ethylene, and xenon near the water critical region, the maximum partial molal volume is approximately 3000 cm^3/mole. A single hydrophobic molecule displaces approximately 40 water molecules. The solvation structure around ions in supercritical water has been simulated by a number of groups.[12,52−54] For a fixed temperature just above the critical temperature, the first solvation shell around simple ions remains intact down to densities of about 0.2 g/cm^3, as indicated by the strongly peaked radial distribution functions $g(r)$ between solute ions and water.[52] The local density enhancement around ions is expected to be largest in the region of highest solvent compressibility, according to the compressible continuum model of Wood and co-workers.[55,56]

In light of these considerations, it seems reasonable to suppose that near 0.5 g/cm^3 in supercritical water at 380 °C, the repulsive hydrophobic molecules SF_6, O_2, and H atoms begin to segregate into voids between dynamic water clusters. (At the higher densities where isolated clusters cannot really exist, one might envision first the formation of a "sponge-like" topology, with the hydrophobic molecules mostly in the bubbles.) The ions $(e^-)_{aq}$ and $(OH^-)_{aq}$ always remain strongly solvated within water clusters. On average, a potential of mean force develops to prevent reactive contact between the ion and hydrophobic species. As we proceed to lower densities from the density of minimum reaction rate, the solvation shell about the ions must thin. We presume that this reduces the potential of mean force barrier and is responsible for the increase in reaction rates again at lower density. It is interesting to note that the sharp transition, and the minimum in reaction rate, occurs at densities significantly higher than the water compressibility maximum at a given temperature. The local density enhancements commonly discussed in the recent literature almost universally occur on the low-density side of the critical point.[57] It is also interesting to note, in Figure 4, that the transition seems to occur at higher density at lower temperatures. These features of the data remain to be explained quantitatively. However, it is worth pointing out that the "thickness" of our postulated mean force barrier depends on the absolute density, not on the "local density enhancement" relative to the average.

In terms of the practical problem of radiation effects in a supercritical water-cooled nuclear reactor, the observation of increased hydrogen atom yield relative to solvated electrons may be of more importance than the unusual reaction rates. A higher yield of H atoms is itself not terribly surprising. In water vapor, it has always been suggested that yields of H atoms and electrons should be nearly equal,[17,58−61] because, below the ionization threshold, the quantum yield for dissociation into H and OH is

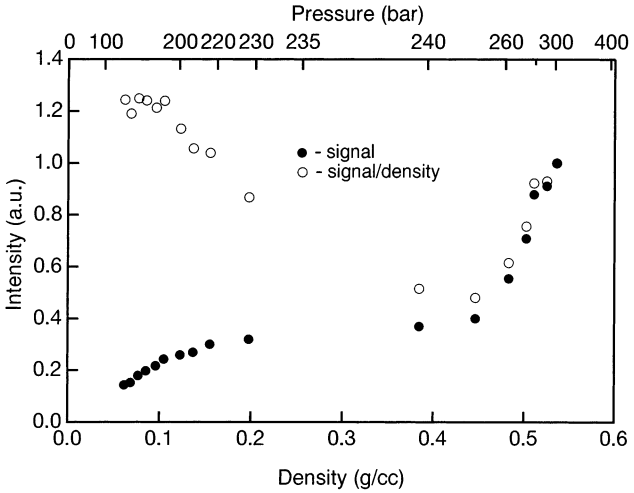

Figure 15. Initial 1200 nm absorption of solvated electrons at 380 °C following 4 ns radiolysis pulses in 0.3 mmolal KOH solution. Filled circles represent the experimental absorption normalized to unity at the highest density. Open circles represent absorption normalized for the water density to give (relative) G_e times ϵ.

essentially unity. The surprise in Figure 13 is that this ratio strongly favors H atoms in supercritical water.

In room-temperature water, the low yield of H atoms relative to solvated electrons is rationalized in terms of several effects.[61] First, the ionization threshold for liquid water is shifted significantly to lower energy relative to the vapor, which favors a higher electron yield. In the vapor, the lowest ionization threshold is at 12.6 eV, but in liquid water the direct ionization pathway seems to begin around 10 eV.[62,63] Second, an efficient mechanism exists whereby water excitons (excited states below 10 eV) can decay to give solvated electrons instead of water dissociation to H and OH.[58,62,63] Third, a major fraction of cage recombination of H and OH can be expected in the liquid. The quantum yield for H atoms in neat water photolysis with 6.7 eV photons is reportedly 0.08,[64,65] implying 90% recombination or radiationless decay. As we lower the density in supercritical water, we can expect all of these condensed phase effects to weaken, so that the G_H/G_e ratio could approach 1.0 as for the isolated H_2O molecule. However, these important effects, taken together, are not sufficient to explain a much higher yield of H than of solvated electrons.

The yield ratio plotted in Figure 13 is a result of the data fitting that includes effects from all of the spur recombination reactions. Relative to lower temperatures, we know that the reaction of solvated electrons with protons to produce H (reaction 8) will be favored by the lower dielectric constant thanks to the Coulombic attraction. At the same time, other major recombination reactions 6 and 4 have a low[46,66] or even negative[26] activation energy. It seems likely that this intraspur charge recombination is an important reason for the increased G_H/G_e ratio as the temperature is raised and the density decreases. It is the only mechanism that can ultimately produce a phenomenological G_H/G_e ratio larger than in the vapor.

A corollary of large G_H/G_e would seem to be a decreased yield of solvated electrons. In Figure 15, we plot the "initial" 1200 nm absorption amplitude of solvated electrons following 4 ns radiolysis pulses in Argon-saturated 0.3 millimolal KOH solution at 380 °C, as a function of the water density. The open circles represent signals divided by the density to normalize for the amount of energy actually absorbed by the sample. Our observations indicate that the spectrum shape is essentially independent of density, for densities greater than 0.2 g/cc. Above 0.2 g/cm^3, the density-normalized points of Figure 15 should therefore be approximately proportional to the yield of electrons, G_e. The electron yield decreases between 0.6 and 0.4 g/cm^3 where we see an increase in G_H/G_e (Figure 13). This is consistent with an increase in G_H at the expense of G_e. However, electron yield increases again between 0.4 and 0.2 g/cc even though G_H/G_e continues to increase. This must indicate an overall increase in the sum of G_H and G_e at low densities. A systematic quantitative study of these yields is planned as a next step in our project.

V. Summary and Conclusions

In summary, we have measured reaction rates for three reactions in supercritical water as a function of the density:

$$(e^-)_{aq} + O_2 \rightarrow O_2^- \quad (11)$$

$$H + OH^- \rightarrow (e^-)_{aq} + H_2O \quad (12)$$

$$(e^-)_{aq} + SF_6 \rightarrow SF_5 + F^- \quad (13a)$$

Although the rate constant and nature of reaction 12 is very different from that of (11) and (13), the effect of density on the rate constant at 380 °C ($T/T_c = 1.01$) is virtually identical for all three reactions. At this temperature, the rates drop very dramatically by a factor of 4 between 0.55 and 0.45 g/cm^3. The rate constants increase again at lower density, regaining the high-density values at 0.1 g/cm^3. The only common characteristic of these three reactions seems to be the involvement of an anion (OH− or $(e^-)_{aq}$) and a hydrophobic molecule (H, SF_6, or O_2). We postulate that the rate constant behavior results from a potential of mean force separating the ion and the hydrophobic species, which for this temperature is always maximized at about 0.45 g/cm^3.

A surprising second result of these experiments is the strong dependence on density of the relative radiolysis yields of H and $(e^-)_{aq}$. Below 300 °C, the ratio G_H/G_e remains about 0.25, but it increases to 0.85 at 350 °C. In the supercritical fluid at 380 °C, the ratio is greater than unity. At lower densities around 0.1 g/cc, the ratio reaches 4.0−6.0. We postulate that this number becomes larger than unity because of the fast charge recombination of electrons and protons in spurs, taken together with increased cage escape of H and OH from water dissociation. Indications are that the sum ($G_H + G_e$) increases significantly in low-density supercritical fluid.

Acknowledgment. We thank Dr. Sergey Chemerisov for his help in running and maintaining the linac accelerator used in this work. We thank Dr. Craig Stuart and Dr. David McCracken of AECL for sharing unpublished data and for useful advice and discussions. K.T. and J.A.C. have been fully supported under NERI Grant No. M9SF99-0276. The submitted manuscript has been authored by a contractor of the U.S. Government under Contract No. W-31-109-ENG-38. Accordingly, the U.S. Government retains a nonexclusive, royalty-free license to publish or reproduce the published form of this contribution or allow others to do so, for U.S. Government purposes.

Supporting Information Available: Tables S1 and S2 contain rate constants for reactions 11−13 and the fitted ratio G_H/G_e tabulated for all of the water P,T state points examined. This material is available free of charge via the Internet at http://pubs.acs.org.

References and Notes

(1) Oka, Y.; Koshizuka, C. *Prog. Nucl. Energy* **1998**, *32*, 163.

(2) Bushby, S. J.; Dimmick, G. R.; Duffey, R. B.; Burrill, K. A.; Chan, P. S. W. *Conceptual designs for advanced, high-temperature CANDU reactors*; ICONE 8: 8th International Conference on Nuclear Engineering, Baltimore, MD, 2000.

(3) SCR2000. *Proceedings of The First International Symposium on Supercritical Water-cooled Reactors, Design and Technology*; The First International Symposium on Supercritical Water-cooled Reactors, Design and Technology, Tokyo, Japan, 2000.

(4) EPRI. *Proceedings: 1989 Workshop on LWR Radiation Water Chemistry and Its Influence on In−Core Structural Materials*; Workshop on LWR Radiation Water Chemistry and Its Influence on In−Core Structural Materials, 1989.

(5) Cohen, P. *Water Coolant Technology of Power Reactors*; Gordon and Breach: New York, 1969.

(6) Roberts, C. B.; Zhang, J. W.; Brennecke, J. F.; Chateauneuf, J. E. *J. Phys. Chem.* **1993**, *97*, 5618.

(7) Mizan, T. I.; Savage, P. E.; Ziff, R. M. *J. Phys. Chem.* **1996**, *100*, 403.

(8) Roberts, C. B.; Brennecke, J. F.; Chateauneuf, J. E. *J. Chem. Soc., Chem. Commun.* **1993**, 868.

(9) Roek, D. P.; Kremer, M. J.; Roberts, C. B.; Chateauneuf, J. E.; Brennecke, J. F. *Fluid Phase Equilib.* **1999**, *160*, 713.

(10) Savage, P. E.; Gopalan, S.; Mizan, T. I.; Martino, C. J.; Brock, E. E. *AIChE J.* **1995**, *41*, 1723.

(11) Westacott, R. E.; Johnston, K. P.; Rossky, P. J. *J. Am. Chem. Soc.* **2001**, *123*, 1006.

(12) Flanagin, L. W.; Balbuena, P. B.; Johnston, K. P.; Rossky, P. J. *J. Phys. Chem. B* **1997**, *101*, 7998.

(13) Goodyear, G.; Maddox, M. W.; Tucker, S. C. *J. Phys. Chem. B* **2000**, *104*, 6240.

(14) Goodyear, G.; Maddox, M. W.; Tucker, S. C. *J. Phys. Chem. B* **2000**, *104*, 6258.

(15) Goodyear, G.; Maddox, M. W.; Tucker, S. C. *J. Chem. Phys.* **2000**, *112*, 10327.

(16) Bartels, D. M.; Cline, J. A.; Jonah, C. D.; Takahashi, K. *J. Phys. Chem. A* **2002**, *106*, 12270.

(17) Draganic, I. G.; Draganic, Z. D. *The Radiation Chemistry of Water*; Academic Press: New York, 1971.

(18) Spinks, J. W. T.; Woods, R. J. *An Introduction to Radiation Chemistry*, 3rd ed.; Wiley-Interscience, New York, 1990.

(19) Pimblott, S. M.; LaVerne, J. A.; Mozumder, A. *J. Phys. Chem.* **1996**, *100*, 8595.

(20) Pimblott, S. M.; LaVerne, J. A. *J. Phys. Chem. A* **1997**, *101*, 5828.

(21) Laverne, J. A.; Pimblott, S. M. *J. Phys. Chem.* **1993**, *97*, 3291.

(22) Pimblott, S. M.; Laverne, J. A. *J. Phys. Chem.* **1994**, *98*, 6136.

(23) McCracken, D. R.; Rasewych, J. B.; Shorter, W. R. *Coolant Radiolysis and Boiling in Water-Cooled Reactors*; Water Chemistry of Nuclear Reactor Systems 5, 1989, London.

(24) Elliot, A. J. *Rate Constants and G-Values for the Simulation of the Radiolysis of Light Water over the Range 0−300 °C*; report AECL-11073, Atomic Energy of Canada, Ltd., 1994.

(25) Elliot, A. J.; Ouellette, D. C.; Stuart, C. R. *The Temperature Dependence of the Rate Constants and Yields for the Simulation of the Radiolysis of Heavy Water*; report AECL-11658, Atomic Energy of Canada, Ltd., 1996.

(26) Christensen, H.; Sehested, K. *J. Phys. Chem.* **1986**, *90*, 186.

(27) Han, P.; Bartels, D. M. *J. Phys. Chem.* **1990**, *94*, 7294.

(28) Han, P.; Bartels, D. M. *J. Phys. Chem.* **1992**.

(29) Durrant, P. J.; Durrant, B. *Introduction to Advanced Inorganic Chemistry*, 2nd ed.; John Wiley & Sons: New York, 1962.

(30) Asmus, K.-D.; Gruenbein, W.; Fendler, J. H. *J. Am. Chem. Soc.* **1970**, *92*, 2625.

(31) Takahashi, K.; Cline, J. A.; Bartels, D. M.; Jonah, C. D. *Rev. Sci. Instrum.* **2000**, *71*, 3345.

(32) Hart, E. J.; Anbar, M. *The Hydrated Electron*; Wiley-Interscience: New York, 1970.

(33) Wu, G.; Katsumura, Y.; Muroya, Y.; Li, X.; Terada, Y. *Chem. Phys. Lett.* **2000**, *325*, 531.

(34) Bartels, D. M.; Cook, A. R.; Mudaliar, M.; Jonah, C. D. *J. Phys. Chem. A* **2000**, *104*, 1686.

(35) Cline, J. A.; Bartels, D. M.; Jonah, C. D. *Rev. Sci. Instrum.* **2002**, *73*, 3908.

(36) Cosgrove, B. A.; Walkley, J. *J. Chromatogr.* **1981**, *216*, 161.

(37) Haar, L.; Gallagher, J. S.; Kell., G. S. *NBS/NRC Steam Tables*; Hemisphere Publishing Corp., 1984.

(38) Ho, P. C.; Palmer, D. A.; Wood, R. H. *J. Phys. Chem. B* **2000**, *104*, 12084.

(39) Majer, V.; Wood, R. H. *J. Chem. Thermodyn.* **1994**, *26*, 1143.

(40) Takahashi, K.; Bartels, D. M.; Cline, J. A.; Jonah, C. D. *Chem. Phys. Lett.* **2002**, *357*, 358.

(41) Asmus, K.-D.; Fendler, J. H. *J. Phys. Chem.* **1968**, *72*, 4285.

(42) Ghandi, K.; Addision-Jones, B.; Brodovitch, J.-C.; McKenzie, I.; Schuth, J.; Percival, P. W. unpublished results summarized in *TRIUMF Annual Report of Scientific Activities 1999*; TRIUMF, Vancouver, BC, 1999; p 65.

(43) Shiraishi, H.; Sunaryo, G. R.; Ishigure, K. *J. Phys. Chem.* **1994**, *98*, 5164.

(44) Schmidt, K. H.; Han, P.; Bartels, D. M. *J. Phys. Chem.* **1995**, *99*, 10530.

(45) *Diffusion-Limited Reactions*; Rice, S. A., Ed.; Elsevier: Amsterdam, 1985; Vol. 25, p 404.

(46) Elliot, A. J.; McCracken, D. R.; Buxton, G. V.; Wood, N. D. *J. Chem. Soc., Faraday Trans.* **1990**, *86*, 1539.

(47) Ibuki, K.; Ueno, M.; Nakahara, M. *J. Phys. Chem. B* **2000**, *104*, 5139.

(48) Tucker, S. C.; Maddox, M. W. *J. Phys. Chem. B* **1998**, *102*, 2437.

(49) Maddox, M. W.; Goodyear, G.; Tucker, S. C. *J. Phys. Chem. B* **2000**, *104*, 6248.

(50) Petsche, I. B.; Debenedetti, P. G. *J. Phys. Chem.* **1991**, *95*, 386.

(51) Biggerstaff, D. R.; Wood, R. H. *J. Phys. Chem.* **1988**, *92*, 1988.

(52) Hyun, J.-K.; Johnston, K. P.; Rossky, P. J. *J. Phys. Chem. A* **2001**, submitted.

(53) Lee, S. H.; Cummings, P. T. *J. Chem. Phys.* **2000**, *112*, 864.

(54) Rasaiah, J. C.; Noworyta, J. P.; Koneshan, S. *J. Am. Chem. Soc.* **2000**, *122*, 11182.

(55) Wood, R. H.; Quint, J. R.; Grolier, J.-P. E. *J. Phys. Chem.* **1981**, *85*, 3944.

(56) Quint, J. R.; Wood, R. H. *J. Phys. Chem.* **1985**, *89*, 380.

(57) Tucker, S. C. *Chem. Rev.* **1999**, *99*, 391.

(58) Han, P.; Bartels, D. M. *J. Phys. Chem.* **1990**, *94*, 5824.

(59) Kaplan, I. G.; Miterev, A. M.; Sukhonosov, V. Y. *Radiat. Phys. Chem.* **1986**, *27*, 83.

(60) Paretzke, H. G.; Turner, J. E.; Hamm, R. N.; Wright, H. A.; Ritchie, R. H. *J. Chem. Phys.* **1986**, *84*, 3182.

(61) Sukhonosov, V. Y. *High Energy Chem.* **1995**, *29*, 243.

(62) Bartels, D. M.; Crowell, R. A. *J. Phys. Chem. A* **2000**, *104*, 3349.

(63) Crowell, R. A.; Bartels, D. M. *J. Phys. Chem.* **1996**, *100*, 17940.

(64) Boyle, J. W.; Ghormley, J. A.; Hochanadel, C. J.; Riley, J. F. *J. Phys. Chem.* **1969**, *73*, 2886.

(65) Sokolov, U.; Stein, G. *J. Chem. Phys.* **1966**, *44*, 3329.

(66) Elliot, A. J.; Ouellette, D. C. *J. Chem. Soc., Faraday Trans.* **1994**, *90*, 837.